

Symmetry breaking and physical properties of the bosonic single-impurity Anderson model

Jesus Herazo Warnes and E. Miranda

Instituto de Física Gleb Wataghin, Rua Sérgio Buarque de Holanda, 777, CEP 13083-859 Campinas, SP, Brazil

We show how exact diagonalization of small clusters can be used as a fast and reliable impurity solver by determining the phase diagram and physical properties of the bosonic single-impurity Anderson model. This is specially important for applications which require the solution of a large number of different single-impurity problems, such as the bosonic dynamical mean field theory of disordered systems. In particular, we investigate the connection between spontaneous global gauge symmetry breaking and the occurrence of Bose-Einstein condensation (BEC). We show how BEC is accurately signaled by the appearance of broken symmetry, even when a fairly modest number of states is retained. The occurrence of symmetry breaking can be detected both by adding a small conjugate field or, as in generic quantum critical points, by the divergence of the associated phase susceptibility. Our results show excellent agreement with the considerably more demanding numerical renormalization group (NRG) method. We also investigate the mean impurity occupancy and its fluctuations, identifying an asymmetry in their critical behavior across the quantum phase transitions between BEC and ‘Mott’ phases.

PACS numbers: 67.85.Bc, 67.85.Jk, 37.10.Gh

I. INTRODUCTION

Strongly correlated impurity models have played an important role in the field of condensed matter physics. The Anderson [1] and the Kondo [2] single-impurity models were at the heart of the early investigations into the formation of localized magnetic moments in metals and their effects on thermodynamic and transport properties of these materials. An extensive arsenal of theoretical techniques have been developed in an effort to better elucidate these and related questions [3] and a great deal of understanding has been thereby achieved. More recently, important methods for the study of *periodic* strongly correlated systems have been developed, such as the dynamical mean field theory (DMFT) [4] and its extensions, which rely heavily on the knowledge base accumulated in the analysis of the aforementioned impurity models. Indeed, solving a single-impurity problem is the most challenging part of the DMFT algorithm.

Since the advent of the possibility of loading extremely cold atoms onto the effective periodic potential formed by optical lattices [5, 6] there has been a growing interest in the cross fertilization between these atomic systems and their conventional condensed matter counterparts. For one thing, cold atoms in optical lattices are expected to be very well described by the simplified models used in the condensed matter context, such as the Hubbard model [6]. For solids, by contrast, these models are believed to be at best a bare bones description which hopefully retains the most important physical features. Moreover, the parameters in cold-atom optical lattice systems, such as hopping amplitudes and scattering lengths can often be very flexibly tuned externally, allowing for the thorough investigation of large portions of the phase diagrams. Finally, the quantum statistics can also be switched as bosonic atoms are readily available.

This fruitful interplay between these condensed mat-

ter and cold-atom systems has prompted researchers to attempt to use impurity-model-based approaches as an analytical tool for cold-atom systems. In particular, the bosonic version of the dynamical mean field theory (BDMFT) has been developed [7–9]. In close analogy with its fermionic counterpart, this method requires the solution of a bosonic single-impurity Anderson model (B-SIAM). This model has been directly studied by the powerful Wilson numerical renormalization group (NRG) technique and its phase diagram has been determined [10, 11]. Furthermore, applications of BDMFT have also been carried out, using as impurity solvers exact diagonalization [12, 13] and quantum Monte Carlo [9, 14]. It should also be mentioned that impurity-like cold-atom set-ups have been proposed [15] and may also become available (for a realization in which *different* species occupy the impurity and the bath regions, see [16]), in which case some version of the single-impurity model may be directly applicable.

More recently, it has become possible to introduce quenched disorder into optical lattice systems [17–26], which may prove useful for the important problem of the interplay between disorder and interactions [27]. The extension of the BDMFT to the disordered case [28], however, requires the solution of a large number of different single-impurity problems for the description of a single disordered sample, as many as the number of lattice sites (for a description of the fermionic version, see [29]). This makes it all but impossible to use such numerically demanding single-impurity solvers as the NRG. Therefore, the feasibility of using the BDMFT to study disordered systems requires the development and characterization of fast yet reliable single-impurity solvers.

One of the goals of this article is to show that the exact diagonalization of small clusters is a good solution to this problem, a procedure which has been successfully applied to the fermionic case [30, 31]. We will show that

it can be efficiently and reliably implemented to solve the B-SIAM by studying its ground state properties. Moreover, with an eye towards its application in a BDMFT calculation, we have thoroughly investigated the appearance of Bose-Einstein condensation (BEC) in this model as a manifestation of the phenomenon of global gauge symmetry breaking. Indeed, the B-SIAM is perhaps the simplest model in which this phenomenon occurs and its reduced Hilbert space provides a unique setting in which to numerically study it. Although this is the standard criterion for the detection of BEC, it was not used in the NRG analysis of the model [10, 11]. The same BEC identification which we will show can be done in the B-SIAM will be useful in the analogous task in a BDMFT calculation. Besides, the B-SIAM has extended regions in which BEC is present or absent (the so-called ‘Mott’ phase) even at zero temperature, with quantum phase transitions between them. We will show how global gauge symmetry breaking can be used to analyze this quantum phase transition in a manner analogous to more conventional systems such as magnetic ones, even though the system sizes used are fairly modest.

We should stress that the question of the best or even the correct criterion for the occurrence of BEC is not devoid of a certain controversy. Indeed, while the existence of a macroscopic eigenvalue of the one-particle density matrix seems to be uncontested as a necessary and sufficient condition for a BEC [32], some objections have been raised, particularly by Leggett [33], as to whether the frequently used (particularly in the condensed matter literature) criterion of “spontaneously broken gauge symmetry” is an adequate alternative. Much of Leggett’s objection seems to be aimed at the *physical basis* of the infinitesimal symmetry-breaking field usually employed in this criterion, rather than at the validity of the *mathematical procedure* it is based upon. Since our main interest here is to show that this criterion is perfectly adequate for a *numerical* investigation of the less studied case of an impurity model, we should be quite safe. Furthermore, it seems clear that, at least in the case of unfragmented condensates, the criterion of a spontaneously broken gauge symmetry is both a sufficient and a necessary condition for Bose-Einstein condensation in bosonic systems (for a specific discussion and review, see [34]).

We will show in this article that, even in fairly small clusters with a restricted number of bosonic states, a detailed characterization of the spontaneously broken gauge symmetry of the BEC phase and an accurate determination of the full phase diagram is possible, which is in excellent agreement with the much more demanding numerical renormalization group method. Furthermore, we will analyze how the impurity occupancy and its fluctuations behave within the phases and through the quantum phase transitions between them. In particular, we pinpoint a qualitative difference in the critical behavior of both of these quantities as one crosses the boundary from BEC to ‘Mott’ as compared to going from ‘Mott’ to BEC.

The paper is divided as follows. Section II is devoted

to the definition of the model and a summary of known results for the non-interacting as well as the interacting cases. Section III expounds on the criterion of global gauge symmetry breaking as a hallmark of BEC. Details of the numerical procedure are explained in Section IV. Results on the symmetry breaking occurring in the model are presented in Section V A, whereas other local impurity properties are shown in Section V B. We draw some final conclusions in Section VI. Some results for the non-interacting limit are relegated to an Appendix.

II. THE BOSONIC SINGLE-IMPURITY ANDERSON MODEL

We will focus our attention on the bosonic version of the single-impurity Anderson model Hamiltonian

$$H = \varepsilon_0 \hat{n}_0 + \frac{1}{2} U \hat{n}_0 (\hat{n}_0 - 1) + \sum_{k \neq 0} \varepsilon_k b_k^\dagger b_k + \sum_{k \neq 0} V_k (b_k^\dagger b_0 + b_0^\dagger b_k). \quad (2.1)$$

Here, b_k are bosonic annihilation operators for the impurity ($k = 0$) and “bath” orbitals ($k \neq 0$), $\hat{n}_0 = b_0^\dagger b_0$ is the number operator for the impurity, ε_0 is impurity single-particle energy, and U measures the interaction strength between bosons inside the impurity orbital. The next two terms of the Hamiltonian describe, respectively, the bath single-particle orbital energies ε_k and the hybridization between impurity and bath states, which occurs with amplitude $V_k \in \mathbb{R}$. We will work in the grand-canonical ensemble at zero temperature and fixed chemical potential μ . All the single-particle energies in Equation (2.1) are assumed to be measured with respect to μ .

Evidently, the physics of the model is strongly dependent on the spectral properties of the bosonic bath. It is common practice, particularly in the quantum dissipation literature, to assume a “soft-gap” spectral function for the bath [35]. A power-law dependence is usually considered [10, 11, 35], such that if

$$\Delta(\omega - i\delta) \equiv \sum_k \frac{V_k^2}{\omega - i\delta - \varepsilon_k}, \quad (2.2)$$

then

$$\text{Im}\Delta(\omega - i\delta) = \pi \sum_k V_k^2 \delta(\omega - \varepsilon_k) \quad (2.3)$$

$$= 2\pi\alpha\omega_c^{1-s}\omega^s\Theta(\omega) \Theta(\omega_c - \omega), \quad (2.4)$$

where ω_c is a frequency cutoff, α plays the role of a dimensionless coupling constant and $\Theta(x)$ is the Heaviside step function. The so-called ohmic case corresponds to $s = 1$, whereas $s < 1$ (> 1) corresponds to the sub-ohmic (super-ohmic) regime.

It is useful to consider first the non-interacting limit, $U = 0$. In this case, the problem can be immediately diagonalized (see the appendix A). The spectrum E_n can

be obtained, e.g., from the impurity site Green's function, and it consists of the roots of the equation

$$E_n - \varepsilon_0 = \sum_k \frac{V_k^2}{E_n - \varepsilon_k} = \Delta(E_n). \quad (2.5)$$

In the case of a power-law bath spectral function there is a critical coupling constant $\alpha_c^0 = s\varepsilon_0/2\omega_c$ (for $s > 0$), such that there appears a vanishing root $E_0 = 0$ for $\alpha = \alpha_c^0$ but not for $\alpha < \alpha_c^0$, as shown in the Appendix. At this point, the lowest state of the system is macroscopically occupied, signaling the phenomenon of Bose-Einstein condensation. Further increase of α renders the system ill-defined (in the grand-canonical ensemble assumed here), since the lowest state falls below the chemical potential ($E_0 < 0$).

At finite U , the BEC only occurs for $0 < s < 1$ [10, 11]. In this case, for coupling constant values $\alpha < \alpha_c(\varepsilon_0, U)$, there is a phase in which the BEC is absent. This phase is adiabatically connected to its $\alpha = 0$ counterpart, in which the impurity is decoupled from the bath and which is characterized by an integer occupation of the impurity site. This is very reminiscent of the Mott insulating phases of the Bose-Hubbard model, hence the name ‘‘Mott phase’’. It should be emphasized, however, that if $\alpha \neq 0$ the impurity occupation deviates from integer values and, in contrast to the Mott insulating case, it does not exhibit plateaus of constant $\langle \hat{n}_0 \rangle$ as a function of ε_0 (see Section V B below). Therefore, this terminology is used in a loose sense. The BEC phase is absent for $s > 1$ [10, 11].

In the NRG study of references [10, 11], the transition from the BEC to the Mott phase was identified from the vanishing of a gap in the spectrum of low-lying excitations. Indeed, much like in the $U = 0$ limit, the splitting-off of an isolated pole from the continuum signals the BEC. We will here, however, explore the criterion of the spontaneous breaking of the (global) gauge symmetry as an alternative signature of this quantum phase transition, in perfect analogy with the case of extended bosonic systems.

III. SPONTANEOUS SYMMETRY BREAKING

We now discuss how to look for the BEC phase transition using the criterion of spontaneously broken gauge symmetry. The original Hamiltonian (2.1) is invariant under the following global gauge transformation

$$b_k \rightarrow e^{i\alpha} b_k, \quad (3.1)$$

which simply reflects the conservation of total particle number $\hat{N} = \sum_k b_k^\dagger b_k$. In order to investigate the spontaneous breaking of this symmetry, one usually introduces a small symmetry breaking field conjugate to the order parameter. In the BEC case, the latter can be taken to be $\langle b_0 \rangle$. We thus modify the Hamiltonian of Equation

(2.1) as follows ($\varphi \in \mathbb{R}$)

$$H \rightarrow H + \varphi (b_0^\dagger + b_0). \quad (3.2)$$

The spontaneous symmetry breaking is signaled by a non-zero value of the following limit

$$\lim_{\varphi \rightarrow 0} \lim_{N \rightarrow \infty} \frac{1}{N} |\langle b_0 \rangle|^2 \neq 0. \quad (3.3)$$

(and it is a necessary and sufficient condition for the existence of BEC [34]). In Equation (3.3), $N = \langle \hat{N} \rangle$.

This can be illustrated in the somewhat artificial non-interacting limit. In this case,

$$H = \varepsilon_0 b_0^\dagger b_0 + \varphi (b_0^\dagger + b_0) + \sum_k \varepsilon_k b_k^\dagger b_k + \sum_k V_k (b_k^\dagger b_0 + b_0^\dagger b_k). \quad (3.4)$$

Using the results of the Appendix, it can be shown that the ground state expectation values are

$$\langle b_0 \rangle = \frac{\varphi}{\kappa}, \quad (3.5)$$

$$\langle b_k \rangle = -\frac{V_k \varphi}{\varepsilon_k \kappa}, \quad (3.6)$$

where

$$\kappa = \sum_k \frac{V_k^2}{\varepsilon_k} - \varepsilon_0. \quad (3.7)$$

We note that the BEC is signaled by the vanishing of the lowest single-particle energy E_0 (when measured with respect to the chemical potential). From Equation (2.5), it is clear that when $E_0 \rightarrow 0$,

$$\kappa \rightarrow 0, \quad (3.8)$$

and the order parameter $\langle b_0 \rangle$ as a function of φ has a diverging slope as a $\varphi \rightarrow 0$, such that it tends to a constant in the BEC. Besides, the total number of bosons is given by (Appendix)

$$N = \left(1 + \sum_k \frac{V_k^2}{\varepsilon_k^2} \right) \frac{\varphi^2}{\kappa^2}. \quad (3.9)$$

The limit of Equation (3.3) in this case is given by

$$\lim_{\varphi \rightarrow 0} \lim_{N \rightarrow \infty} \frac{1}{N} |\langle b_0 \rangle|^2 = \left(1 + \sum_k \frac{V_k^2}{\varepsilon_k^2} \right)^{-1} < 1. \quad (3.10)$$

IV. NUMERICAL METHOD

We now describe the numerical procedure used in the calculations that follow. The Hamiltonian of Equation

(2.1) will now be defined with a finite number N_s of bath states

$$H = \varepsilon_0 \hat{n}_0 + \frac{1}{2} U \hat{n}_0 (\hat{n}_0 - 1) + \varphi \sum_{n=0}^{N_s} (b_n^\dagger + b_n) + \sum_{n=1}^{N_s} \varepsilon_n b_n^\dagger b_n + \sum_{n=1}^{N_s} V_n (b_n^\dagger b_0 + b_0^\dagger b_n). \quad (4.1)$$

Note that we have already included the symmetry breaking field φ and it now acts on both impurity and bath states. Since the condensation occurs in a single-particle state which is a quantum mixture of all k -orbitals [see Eqs. (A23) and (A24) for the non-interacting case], it is immaterial whether we couple φ to all of them or only to b_0 . Indeed, we have checked that applying φ only to the impurity site does not change the results that follow in any significant way.

The discretized Hamiltonian (4.1) has no conserved quantities since even the total number of bosons is no longer fixed. Since the boson spectrum is unlimited the Hilbert space has infinite dimension. We worked in a cut-off Hilbert space in which there is a maximum number of bosons

$$\sum_{n=0}^{N_s} b_n^\dagger b_n \leq N_{max}. \quad (4.2)$$

We therefore numerically diagonalized the Hamiltonian (4.1) for fixed N_s and N_{max} .

The parameters $\{\varepsilon_n, V_n\}$ uniquely determine the bath spectral function $\text{Im}\Delta(\omega)$, whose support we will assume is the interval $[0, \omega_c]$, see Equation (2.3). Discretizing the latter set into N_s smaller intervals defined by $[a_{n-1}, a_n]$, where $n = 1, 2, \dots, N_s$, and assuming that $\varepsilon_n \in [a_{n-1}, a_n]$ it follows that

$$V_n^2 = \int_{a_{n-1}}^{a_n} \frac{\text{Im}\Delta(x)}{\pi} dx \quad (n = 1, 2, \dots, N_s), \quad (4.3)$$

$$V_n^2 \varepsilon_n = \int_{a_{n-1}}^{a_n} \frac{x \text{Im}\Delta(x)}{\pi} dx \quad (n = 1, 2, \dots, N_s). \quad (4.4)$$

Although the use of a purely logarithmic mesh would have been enough, we have chosen to use a mixed linear-logarithmic set

$$a_n = \frac{n}{N_s} \frac{\omega_c}{\Lambda^{(N_s-n)}}, \quad (n = 0, 1, 2, \dots, N_s). \quad (4.5)$$

It is close to the usual logarithmic discretization of the numerical renormalization group at low energies but does a better job at describing the high-energy part of the bath spectrum. The linear discretization is recovered in the limit $\Lambda \rightarrow 1$. In the calculations that follow, we have used $\Lambda = 2$.

V. RESULTS

We will now show our results for the bosonic single-impurity Anderson model with a power-law spectral function as in Equation (2.3), with $s = 0.4$. This model exhibits two phases: a Bose-Einstein condensed phase (BEC) and a Mott phase, as shown in [10, 11].

A. Symmetry breaking and the phase diagram

We have computed the value of the order parameter $\langle b_0 \rangle$ as a function of the symmetry breaking field φ for a coupling to the bosonic bath of $\alpha\omega_c/U = 0.0625$ and interaction strength $U = 0.5\omega_c$. According to the NRG results [10, 11], for these values of α and U the system may find itself in either the Mott or the BEC phases, depending of the value of ε_0 . As shown in Figure 1, for $\varepsilon_0/U = 0$, $\langle b_0 \rangle$ smoothly extrapolates to zero, with a finite slope, as $\varphi \rightarrow 0$. This is characteristic of a non-condensed phase with no broken global gauge symmetry, the Mott phase of the model. At $\varepsilon_0/U = -0.21$, however, even though $\langle b_0 \rangle$ still vanishes in this limit, it does so with a very large slope, effectively infinite within our numerical accuracy. This signals the boundary with the BEC phase and points to a second order phase transition, consistent with the NRG results [10, 11]. Inside the BEC phase ($\varepsilon_0/U = -0.25$), the superfluid parameter has a step discontinuity (again within our numerical accuracy) across the $\varphi = 0$ line. The similarity with the behavior of a ferromagnet in a uniform external field is striking, highlighting the common underlying symmetry breaking mechanism in both cases.

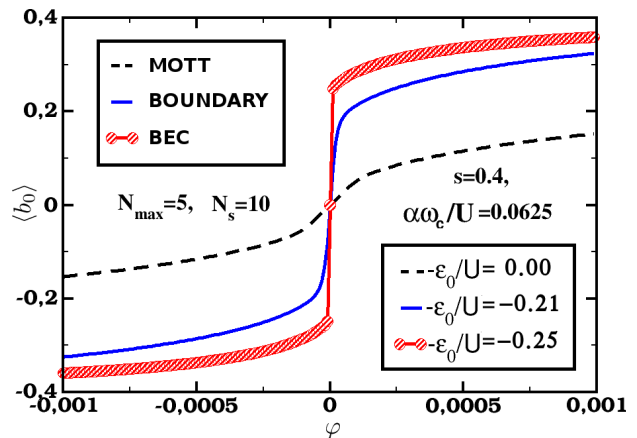


Figure 1. The superfluid order parameter $\langle b_0 \rangle$ as a function of the symmetry breaking field φ for three different values of ε_0/U : the dashed black line ($\varepsilon_0/U = 0$) corresponds to the Mott phase, the red circles ($\varepsilon_0/U = -0.25$) to the BEC phase and the full blue line ($\varepsilon_0/U = -0.21$) to the boundary between the two phases. The slope at $\varphi = 0$ is finite within the Mott phase and infinite at the phase boundary. We have used $N_s = 10$, $N_{max} = 5$, $U = 0.5\omega_c$, $\alpha\omega_c/U = 0.0625$ and $s = 0.4$.

By looking for the points of infinite slope of the $\langle b_0 \rangle$ versus φ curves one can then map out the phase diagram of the model. We have done so in the ε_0 versus α plane for $U = 0.5\omega_c$. In practice, we have set the phase boundary as the point at which the slope reaches 10^4 . The same phase diagram had been previously obtained with the much more powerful NRG method using the ‘gap closure’ criterion (see Section II) [10, 11]. The NRG parameters used were $\Lambda = 2$ (for a purely logarithmic discretization), 10 to 20 bosonic states for each added site/iteration and 100 to 200 states kept from each iteration to the next. In our exact diagonalization method, we have used $N_s = 10 - 20$ and $N_{max} = 2 - 6$. In Figure 2, a comparison between the results obtained with the two methods is shown. Despite the simplicity of the present procedure and small number of states retained, the agreement is remarkable. We have also verified that the susceptibility criterion we used tracks very closely the opening of the gap discussed in Section II. The assignment of average occupations $n_0 = \langle \hat{n}_0 \rangle$ to the phases, as shown in Figure 2, will be discussed later in Sec. V B.

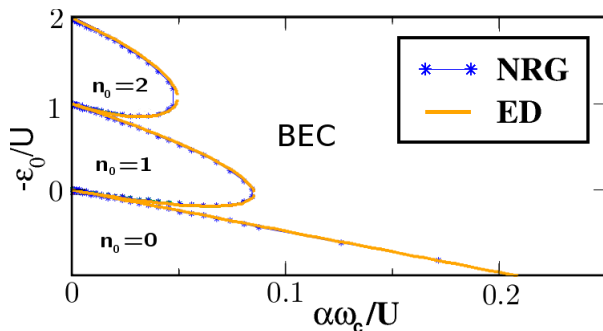


Figure 2. Phase diagram of the bosonic single-impurity Anderson model for $s = 0.4$ and $U/\omega_c = 0.5$ (other parameters as in Figure 1). The blue line with symbols is the phase diagram calculated with the NRG method [10, 11] and the full orange line was determined using the criterion of global gauge symmetry breaking and exact diagonalization. See text for more details.

Another interesting quantity is the phase susceptibility,

$$\chi_\varphi = \lim_{\varphi \rightarrow 0} \frac{\partial |\langle b_0 \rangle|}{\partial \varphi}. \quad (5.1)$$

As discussed in Section III, this quantity is finite in the absence of BEC and diverges at the critical point at which BEC first appears, see Equations (3.5), (3.7) and (3.8). The analogous quantity in the case of a ferromagnet is the magnetic susceptibility, which is also finite in the paramagnetic phase and diverges at the (second-order) phase transition. Thus, we expect χ_φ to be finite in the Mott phase and to diverge at the Mott-BEC boundary. That the transition is indeed second-order was confirmed in Refs. [10, 11]. This behavior is apparently consistent with the gross features of Figure 1, but it is important to

determine how it is affected by our Hilbert space truncation.

In Figure 3(a), we show the inverse phase susceptibility as a function of $1/N_{max}$. It can be seen that χ_φ extrapolates as expected in the limit of $N_{max} \rightarrow \infty$: in the Mott phase ($\varepsilon_0/U = 0$) it tends to a finite value, whereas it diverges at the Mott-BEC boundary (their position in the phase diagram is shown in Figure 3(b)). Note the scale of the figure and how the susceptibility values are significantly different already for the largest modest N_{max} used ($= 6$). Note that the dependence on N_s is extremely weak, since it modifies only slightly the single-particle orbital in which the bosons condense, whereas N_{max} limits the maximum number of bosons allowed to condense.

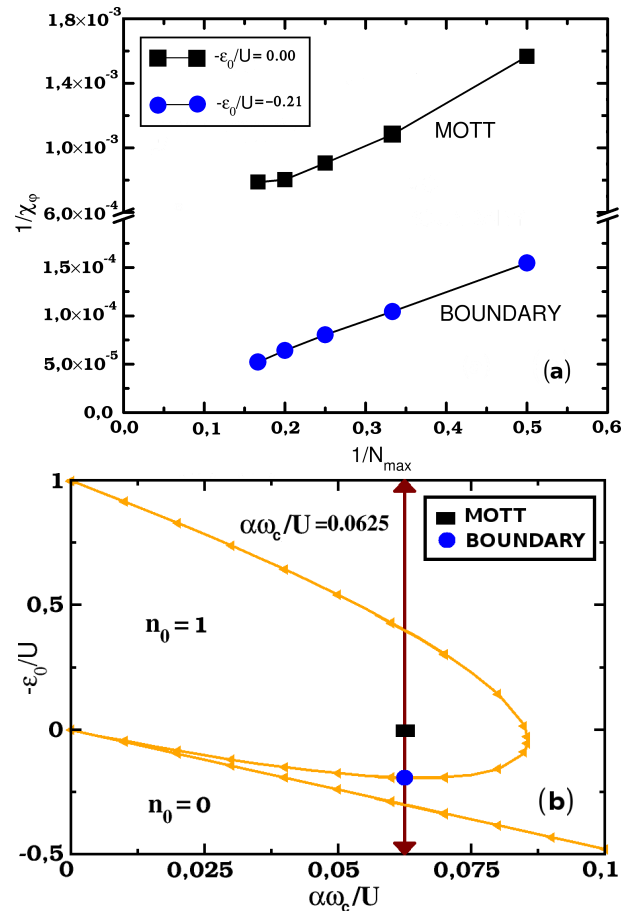


Figure 3. (a) Phase susceptibility as a function of $1/N_{max}$ for two values of ε_0 : for $\varepsilon_0/U = 0$, the system is in the Mott phase and χ_φ extrapolates to a constant when $N_{max} \rightarrow \infty$; the value $\varepsilon_0/U = 0.21$ marks the boundary between Mott and BEC phases and correspondingly gives to a divergent χ_φ in the limit of infinite N_{max} . Other parameters are the same as in Figure 1. (b) Position in the phase diagram of the parameters in (a).

The great differences in susceptibility values allow us to determine the phase diagram with fairly good accuracy also by fixing φ at a small value, say $\sim 10^{-6}$, and N_{max} to a moderately large, yet numerically feasible value of

5, and scanning ε_0 and α . As an example of this procedure, we show in Figure 4(a) the order parameter as a function of ε_0 for fixed α (this corresponds to the brown vertical line of Figure 3(b)). The BEC phase is clearly demarcated from the Mott phase by a finite value of the order parameter. Note, however, that the actual numerical value of $\langle b_0 \rangle$ is strongly dependent on the truncation parameter N_{max} . Indeed, this is clearly demonstrated in Figure 4(b), which shows a similar scan of ε_0 for different values of N_{max} . For small values of N_{max} the order parameter shows pronounced peaks close to the phase boundaries but dips to smaller values deep inside the BEC phase. Only for sufficiently large N_{max} does one recover the single hump behavior of $\langle b_0 \rangle$, with a maximum value deep inside the BEC phase. Note that the criterion of a phase susceptibility of 10^4 used in Figure 2 is equivalent to a value of the order parameter of 2.5×10^{-2} in Figure 4(a). This dependence on N_{max} is not unexpected since, as will be shown later, the fluctuations in the occupancy are larger in the BEC phase. Thus, the truncation at a finite value of the total number of bosons introduces important errors and correspondingly larger values of N_{max} are required for a good description in this region. This allows us to estimate the error in the determination of the phase boundary as $\Delta\varepsilon_{0c} \sim 0.05U_0$.

Furthermore, for the value of α used in Figure 4, the system is always in a BEC phase for $-\varepsilon_0/U \gtrsim 0.3$. These large values of $-\varepsilon_0$ give rise to large occupancies of the impurity orbital. As a result, the description in this region is very poor for the values of N_{max} we employed, as can be seen in Figure 4(b).

B. Other observables

As a test of the accuracy of our procedure, we have calculated other local observables of the impurity orbital. Whenever available, we have compared them with the NRG results [10, 11]. In Figure 5, the impurity occupancy ($n_0 = \langle b_0^\dagger b_0 \rangle$) is shown for different values of the coupling to the bosonic bath as a function of ε_0 . Our results are the full lines and the NRG results [10] correspond to the symbols. The regions without any symbol indicate the BEC phases. The agreement is excellent and one can hardly distinguish the two sets of results. As the coupling α to the bosonic bath decreases, the occupancy tends smoothly to the step-like behavior of the decoupled impurity, also shown Figure 5 (blue line). It is this ‘adiabatic’ continuity between the Mott phases at $\alpha = 0$ and $\alpha \neq 0$ which allows us to ascribe a definite occupancy to the Mott ‘lobes’ of the phase diagram (see Figure 2), even though the occupancy is never exactly an integer for $\alpha > 0$, as can be seen in Figure 5. The excellent agreement shows that our truncated Hilbert space calculation is more than enough for a good description of at least some of the physical properties of the impurity model.

For completeness, in Figure 6 we show our results for both the impurity occupancy (symbols) and the order

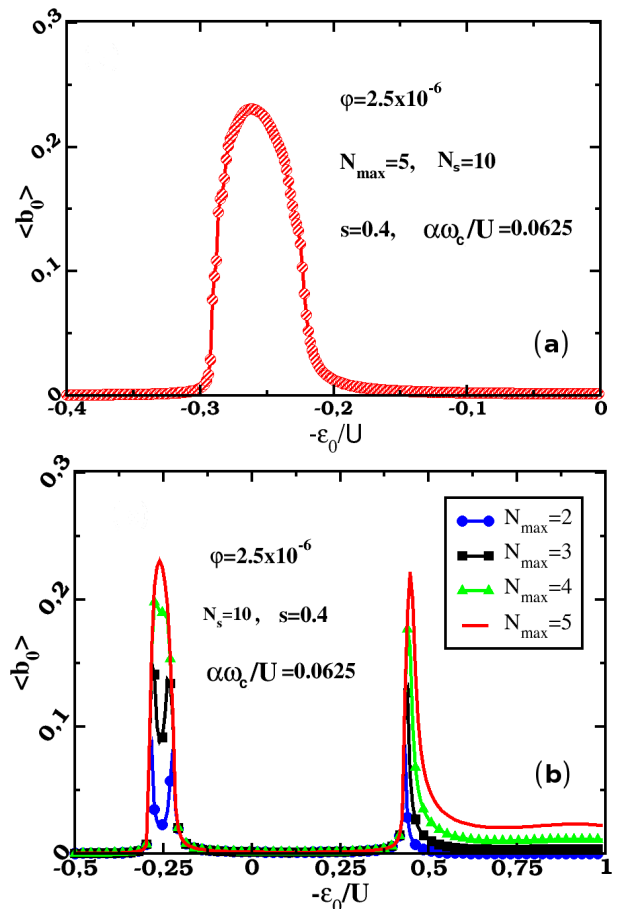


Figure 4. Behavior of the order parameter $\langle b_0 \rangle$ for a fixed small symmetry breaking field ($\varphi \sim 10^{-6}$) in the different phases. (a) $\langle b_0 \rangle$ is finite inside the BEC phase but negligibly small within the Mott phase; (b) the actual value of $\langle b_0 \rangle$ is strongly dependent on the truncation parameter N_{max} within the BEC phase. Other parameters are the same as in Figure 1.

parameter squared (full line without symbols) as functions of ε_0/U , both in the presence of a small symmetry-breaking field. We have rescaled $|\langle b_0 \rangle|^2$ by a factor of ten for greater clarity. It is clear that the small symmetry-breaking field, although essential to delineate the phases, affects very little the impurity occupancy (compare with Figure 5). In this figure, the absence of symbols in the BEC region is meant to mimic the convention for this phase used in the NRG calculation [10] (see Figure 5 for comparison).

Another striking feature highlighted in Figure 6 is the discrepant behavior of the impurity occupancy at the two borders of the BEC phase. Whereas at the low $-\varepsilon_0$ border n_0 exhibits a discontinuity in its first derivative, the behavior at the high $-\varepsilon_0$ border is perfectly smooth. This behavior is generic to all the other BEC phases, as can be seen in Figure 5. We conclude that although n_0 shows signs of critical behavior at the low $-\varepsilon_0$ border of the BEC phases, it is not critical at the other one.

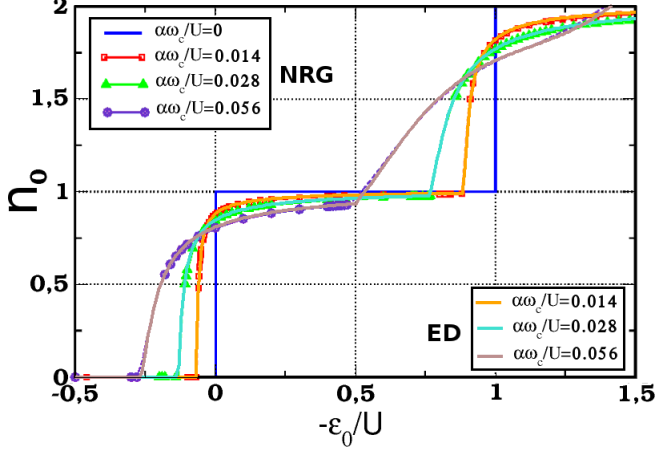


Figure 5. Occupancy of the impurity orbital as a function of ε_0 for different values of α . The symbols are the NRG results of reference [10, 11] and the full lines correspond to our results. The agreement is remarkable. The curves smoothly tend to the step-like behavior of the limit of a decoupled impurity ($\alpha = 0$). Other parameters are the same as in Figure 1.

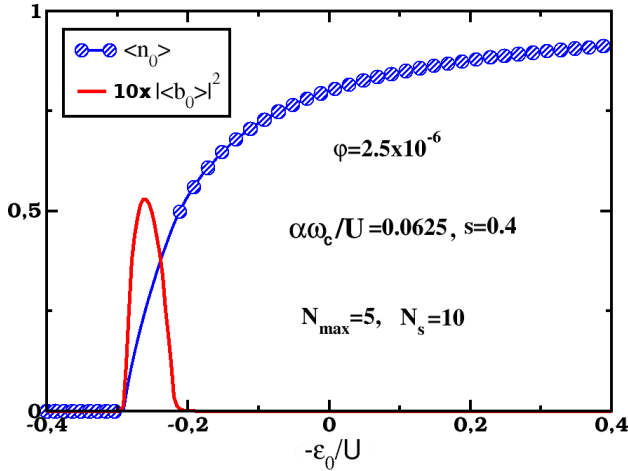


Figure 6. Impurity occupancy and order parameter squared as functions of the impurity single-particle energy ε_0 . The small symmetry breaking field hardly affects the occupancy. Other parameters are the same as in Figure 1.

Finally, in Figure 7(a), we show the impurity occupancy fluctuation $\Delta n_0 = \sqrt{\langle \hat{n}_0^2 \rangle - \langle \hat{n}_0 \rangle^2}$ in the (ε_0, α) plane with a color scale. The borders between the phases are also shown as the blue lines with symbols. Three vertical cuts across this plot are shown in Figure 7(b), with

the BEC region indicated by the closed symbols and the ‘Mott’ phase by the open ones. The occupancy fluctuation is generally larger in the BEC regions as compared to the ‘Mott’ phases, as expected. Indeed, this is compatible with the requirement of larger values of N_{max} for a better description deep within the BEC phases (see Figure 4b).

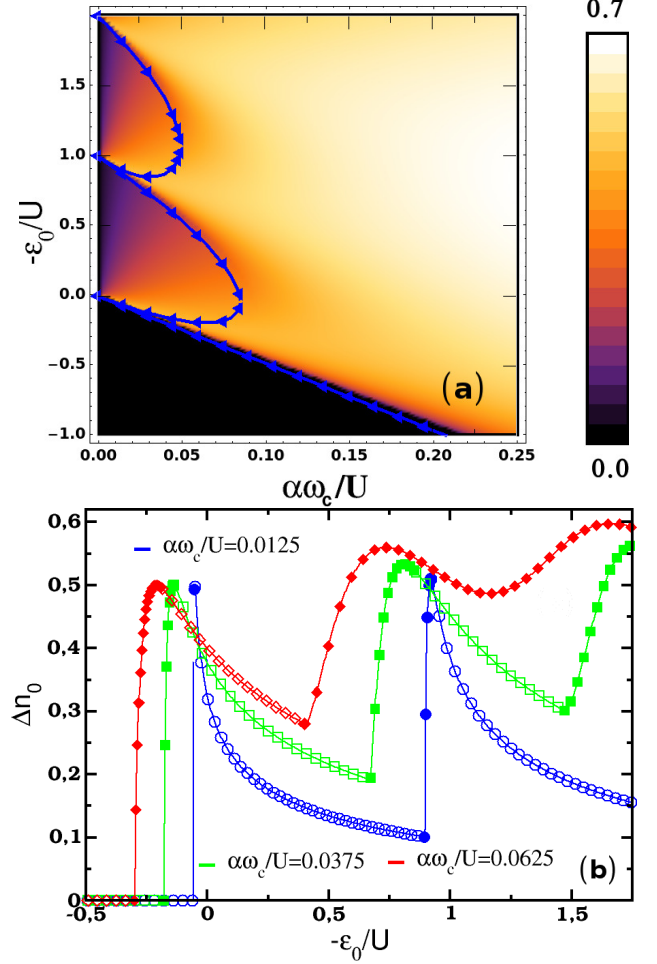


Figure 7. Impurity occupancy fluctuation Δn_0 : (a) in the (ε, α) plane. The full blue line with symbols marks the phase boundaries); (b) as a function of ε_0 for three values of α . The open symbols correspond to the ‘Mott’ phase and closed ones to the BEC. Other parameters are the same as in Figure 1.

However, a more thorough inspection shows that whereas Δn_0 increases rapidly upon entering the BEC phase through its low $-\varepsilon_0$ border, it goes through a maximum while still *inside* the BEC phase. Upon further increasing $-\varepsilon_0$, Δn_0 decreases until it finally crosses the high $-\varepsilon_0$ border of the BEC phase, where it shows no sign of critical behavior, in close similarity with the behavior of n_0 shown in Figure 6. We stress that, even though the high $-\varepsilon_0$ transition does not manifest itself in these quantities, does not mean that the system does not experience a true phase transition in that region. Furthermore, the occupancy fluctuation does not vanish and is always a

monotonically decreasing function of $-\varepsilon_0$ in the ‘Mott’ phases for $n_0 \neq 0$.

VI. DISCUSSION AND CONCLUSIONS

In this article, we have fully characterized the diverse physical properties of the B-SIAM by using the relatively undemanding method of exact diagonalization of small clusters. Besides, we have shown how the physically motivated criterion of a spontaneously broken gauge symmetry can be used to accurately identify the BEC or ‘Mott’ phases of the B-SIAM, even with a fairly small truncated Hilbert space. This serves as a proof of principle of the criterion in this particular case. Clearly, the detailed quantum critical behavior requires the use of many more states, in which case the NRG method is probably indispensable. However, the exact diagonalization method is accurate enough for the determination of phase diagrams and physical properties, as we have shown. This is particularly important for applications such as the disordered version of BDMFT. In these cases, the use of the more accurate NRG method is prohibitive.

We have also uncovered an unnoticed asymmetry in the critical behavior of local quantities as one goes from ‘Mott’ to BEC and BEC to ‘Mott’. In the former case, both the mean occupancy and its fluctuations exhibit a discontinuity in the first derivative with respect to the impurity energy, whereas the latter transition seems to be completely smooth. This is probably a feature of the single-impurity model only, however, since the incompressible nature of the Mott phase in the lattice case requires both borders to show non-analytic behavior. The single-impurity model, on the other hand, is not incompressible in the ‘Mott’ phase.

ACKNOWLEDGMENTS

This work was supported by CNPq through grants 304311/2010-3 (EM) and 140184/2007-4 (JHW) and by FAPESP through grant 07/57630-5 (EM).

Appendix A: General properties of the non-interacting limit

1. Diagonalization of the non-interacting model

We will first briefly describe the diagonalization of the non-interacting Hamiltonian, Equation (2.1) with U set to zero. The absence of interactions makes this process independent of the statistics, since it amounts to finding the basis of single-particle states that makes the Hamiltonian diagonal. A more detailed calculation, in the language of fermions, can be found in reference [36]. We define annihilation operators c_j for the diagonal single-particle states through

$$b_0 = \sum_j \gamma_j c_j, \quad (\text{A1})$$

$$b_k = \sum_j \nu_{kj} c_j, \quad (\text{A2})$$

so that the non-interacting Hamiltonian can be written in this basis as

$$H = \sum_j E_j c_j^\dagger c_j. \quad (\text{A3})$$

The coefficients γ_j and ν_{kj} have yet to be determined. By taking the commutator of b_k and c_j with the Hamiltonian in the forms (2.1) and (A18), respectively, and using (A1) and (A2), we find the eigenvalue system of equations for the unknown coefficients

$$(E_j - \varepsilon_0) \gamma_j = \sum_k V_k \nu_{kj}, \quad (\text{A4})$$

$$(E_j - \varepsilon_k) \nu_{kj} = V_k \gamma_j. \quad (\text{A5})$$

Inserting Equation (A5) into Equation (A4) we obtain an implicit equation for the eigenvalues E_j

$$E_j - \varepsilon_0 = \sum_k \frac{V_k^2}{E_j - \varepsilon_k}. \quad (\text{A6})$$

The normalization condition

$$\gamma_j^2 + \sum_k \nu_{kj}^2 = 1, \quad (\text{A7})$$

together with (A5), leads to

$$\gamma_j^{-2} = 1 + \sum_k \frac{V_k^2}{(E_j - \varepsilon_k)^2}, \quad (\text{A8})$$

and finally Equation (A5) can be used to find an expression for the ν_{kj} coefficients, which we will omit.

2. Critical coupling for a power-law spectral density

The BEC in the non-interacting model occurs when the lowest eigenvalue (measured with respect to the chemical potential) vanishes. From Equation (A6), this happens when

$$\varepsilon_0 = \sum_k \frac{V_k^2}{\varepsilon_k}. \quad (\text{A9})$$

We would like to analyze this equation in the continuum limit. In this case, we can use the function defined in Equation (2.2), which satisfies the Kramers-Kronig relation

$$\text{Re}\Delta(\omega - i\delta) = \mathcal{P} \int \frac{dx}{\pi} \frac{\text{Im}\Delta(x - i\delta)}{\omega - x}, \quad (\text{A10})$$

in which the integral is a principal part. Thus, one may replace the right-hand side of Equation (A9) by

$$\sum_k \frac{V_k^2}{\varepsilon_k} = -\text{Re}\Delta(0 - i\delta) = \int \frac{dx}{\pi} \frac{\text{Im}\Delta(x - i\delta)}{x}.$$

For the power-law spectral function of Equation (2.3), we are left with an expression for the critical coupling α_c^0

$$\varepsilon_0 = 2\alpha_c^0 \omega_c^{1-s} \int_0^{\omega_c} x^{s-1} dx = \frac{2}{s} \alpha_c^0 \omega_c \quad (s > 0).$$

Note that the equation is not well defined for $s \leq 0$. We finally find that

$$\alpha_c^0 = \frac{s\varepsilon_0}{2\omega_c} \quad (s > 0).$$

3. The non-interacting Hamiltonian in the presence of a symmetry-breaking field

We now consider the non-interacting Hamiltonian in the presence of a symmetry-breaking field, Equation (3.4). We first define ‘displaced’ operators a_0 and a_k

$$b_0 = a_0 + \lambda, \quad (\text{A11})$$

$$b_k = a_k + \eta_k, \quad (\text{A12})$$

where the parameters λ, η_k can be taken to be real without loss of generality. Inserting these into (3.4) we end up with

$$\begin{aligned} H = & \varepsilon_0 a_0^\dagger a_0 + \left(\varphi + \lambda\varepsilon_0 + \sum_k \eta_k V_k \right) (a_0^\dagger + a_0) \\ & + \sum_k \varepsilon_k a_k^\dagger a_k + \sum_k (\varepsilon_k \eta_k + \lambda V_k) (a_k^\dagger + a_k) \\ & + \sum_k V_k (a_k^\dagger a_0 + a_0^\dagger a_k) \\ & + \varepsilon_0 \lambda^2 + 2\lambda\varphi + \sum_k \varepsilon_k \eta_k^2 + 2\lambda \sum_k V_k \eta_k. \end{aligned}$$

The terms linear in the new ‘displaced’ operators can be eliminated if we choose λ and η_k to satisfy

$$\varphi + \lambda\varepsilon_0 + \sum_k \eta_k V_k = 0, \quad (\text{A13})$$

$$\varepsilon_k \eta_k + \lambda V_k = 0. \quad (\text{A14})$$

Taking η_k from Equation (A14) into (A13) we find

$$\eta_k = -\lambda \frac{V_k}{\varepsilon_k}, \quad (\text{A15})$$

$$\lambda = \frac{\varphi}{\sum_k \frac{V_k^2}{\varepsilon_k} - \varepsilon_0} \equiv \frac{\varphi}{\kappa}. \quad (\text{A16})$$

For this choice, we are left with

$$H = \varepsilon_0 a_0^\dagger a_0 + \sum_k \varepsilon_k a_k^\dagger a_k + \sum_k V_k (a_k^\dagger a_0 + a_0^\dagger a_k) + \frac{\varphi^2}{\kappa}. \quad (\text{A17})$$

As shown before, the Hamiltonian (A17) can be brought to diagonal form by means of the canonical transformation of Eqs. (A1) and (A2), with γ_j given by (A8) and ν_{kj} given by (A5). Thus,

$$H = \sum_j E_j c_j^\dagger c_j + \frac{\varphi^2}{\kappa}. \quad (\text{A18})$$

where,

$$b_0 = \lambda + \sum_j \gamma_j c_j, \quad (\text{A19})$$

$$b_k = \eta_k + \sum_j \nu_{kj} c_j. \quad (\text{A20})$$

Since the ground state $|\Phi_0\rangle$ is annihilated by the c_j operators it follows that

$$\sum_j \gamma_j c_j |\Phi_0\rangle = (b_0 - \lambda) |\Phi_0\rangle = 0, \quad (\text{A21})$$

$$\sum_j \nu_{kj} c_j |\Phi_0\rangle = (b_k - \eta_k) |\Phi_0\rangle = 0. \quad (\text{A22})$$

Therefore, the expectation values of the b operators in the ground state does not vanish

$$\langle b_0 \rangle = \lambda, \quad (\text{A23})$$

$$\langle b_k \rangle = \eta_k. \quad (\text{A24})$$

Furthermore, the total number of particles is given by

$$N = \langle b_0^\dagger b_0 \rangle + \sum_k \langle b_k^\dagger b_k \rangle = \lambda^2 + \sum_k \eta_k^2. \quad (\text{A25})$$

Using Equations (A15) and (A16)

$$N = \left(1 + \sum_k \frac{V_k^2}{\varepsilon_k^2} \right) \frac{\varphi^2}{\kappa^2}. \quad (\text{A26})$$

[1] P. W. ANDERSON, *Phys. Rev.* **124**, 41 (1961).

[2] J. KONDO, *Prog. Theor. Phys.* **32**, 37 (1964).

- [3] A. C. HEWSON, *The Kondo Problem to Heavy Fermions*, Cambridge University Press, Cambridge, 1993.
- [4] A. GEORGES, G. KOTLIAR, W. KRAUTH, and M. J. ROZENBERG, *Rev. Mod. Phys.* **68**, 13 (1996).
- [5] D. JAKSCH, C. BRUDER, J. I. CIRAC, C. W. GARDINER, and P. ZOLLER, *Phys. Rev. Lett.* **81**, 3108 (1998).
- [6] D. JAKSCH and P. ZOLLER, *Annals of Physics* **315**, 52 (2005).
- [7] K. BYCZUK and D. VOLLHARDT, *Phys. Rev. B* **77**, 235106 (2008).
- [8] M. SNOEK and W. HOFSTETTER, Bosonic Dynamical Mean-Field Theory, in *Quantum gases: Finite Temperature and Non-Equilibrium Dynamics*, edited by N. PROUKAKIS, S. GARDINER, M. DAVIS, N. NYGAARD, and M. SZYMANSKA, Imperial College Press, 2012.
- [9] P. ANDERS, E. GULL, L. POLLET, M. TROYER, and P. WERNER, *New J. of Phys.* **13**, 075013 (2011).
- [10] H.-J. LEE and R. BULLA, *Eur. Phys. J. B* **56**, 199 (2007).
- [11] H.-J. LEE, K. BYCZUK, and R. BULLA, *Phys. Rev. B* **82**, 054516 (2010).
- [12] A. HUBENER, M. SNOEK, and W. HOFSTETTER, *Phys. Rev. B* **80**, 245109 (2009).
- [13] W.-J. HU and N.-H. TONG, *Phys. Rev. B* **80**, 245110 (2009).
- [14] P. ANDERS, E. GULL, L. POLLET, M. TROYER, and P. WERNER, *Phys. Rev. Lett.* **105**, 096402 (2010).
- [15] A. RECATI, P. O. FEDICHEV, W. ZWERGER, J. VON DELFT, and P. ZOLLER, *Phys. Rev. Lett.* **94**, 040404 (2005).
- [16] C. ZIPKES, S. PALZER, C. SIAS, and M. KOHL, *Nature* **464**, 388 (2010).
- [17] P. HORAK, J.-Y. COURTOIS, and G. GRYNBERG, *Phys. Rev. A* **58**, 3953 (1998).
- [18] D. BOIRON, C. MENNERAT-ROBILLIARD, J.-M. FOURNIER, L. GUIDONI, C. SALOMON, and G. GRYNBERG, *Eur. Phys. J. D* **7**, 373 (1999).
- [19] R. B. DIENER, G. A. GEORGAKIS, J. ZHONG, M. RAIZEN, and Q. NIU, *Phys. Rev. A* **64**, 033416 (2001).
- [20] R. ROTH and K. BURNETT, *Phys. Rev. A* **68**, 023604 (2003).
- [21] B. DAMSKI, J. ZAKRZEWSKI, L. SANTOS, P. ZOLLER, and M. LEWENSTEIN, *Phys. Rev. Lett.* **91**, 080403 (2003).
- [22] H. GIMPERLEIN, S. WESSEL, J. SCHMIEDMAYER, and L. SANTOS, *Phys. Rev. Lett.* **95**, 170401 (2005).
- [23] U. GAVISH and Y. CASTIN, *Phys. Rev. Lett.* **95**, 020401 (2005).
- [24] P. MASSIGNAN and Y. CASTIN, *Phys. Rev. A* **74**, 013616 (2006).
- [25] L. FALLANI, J. E. LYE, V. GUARRERA, C. FORT, and M. INGUSCIO, *Phys. Rev. Lett.* **98**, 130404 (2007).
- [26] E. LUCIONI, B. DESSLER, L. TANZI, G. ROATI, M. ZACCANTI, M. MODUGNO, M. LARCHER, F. DALFOVO, M. INGUSCIO, and G. MODUGNO, *Phys. Rev. Lett.* **106**, 230403 (2011).
- [27] P. A. LEE and T. V. RAMAKRISHNAN, *Rev. Mod. Phys.* **57**, 287 (1985).
- [28] For other approaches to the disordered bosonic lattice problem see, e. g., U. BISSBORT, R. THOMALE, and W. HOFSTETTER *Phys. Rev. A* **81**, 063643 (2010) and M. KNAP, E. ARRIGONI, and W. VON DER LINDEN *Phys. Rev. A* **82**, 053628 (2010).
- [29] V. DOBROSAVLJEVIĆ and G. KOTLIAR, *Philos. Trans. R. Soc. London A* **356**, 57 (1998).
- [30] M. CAFFAREL and W. KRAUTH, *Phys. Rev. Lett.* **72**, 1545 (1994).
- [31] H. KAJUETER and G. KOTLIAR, *Phys. Rev. Lett.* **77**, 131 (1996).
- [32] C. N. YANG, *Rev. Mod. Phys.* **34**, 694 (1962).
- [33] A. J. LEGGETT, *Quantum Liquids: Bose condensation and Cooper pairing in condensed-matter systems*, Oxford University Press, 2005.
- [34] V. YUKALOV, *Laser Physics Letters* **4**, 632 (2007).
- [35] A. J. LEGGETT, S. CHAKRAVARTY, A. T. DORSEY, M. P. A. FISHER, A. GARG, and W. ZWERGER, *Rev. Mod. Phys.* **59**, 1 (1987).
- [36] G. D. MAHAN, *Many-Particle Physics*, chapter 4.2, Plenum, 2nd. edition, 1990.